Mon. Not. R. Astron. Soc. **287,** 848–866 (1997)

The Edinburgh–Cape Blue Object Survey – I. Description of the survey

R. S. Stobie,[1] D. Kilkenny,[1] D. O'Donoghue,[2] A. Chen,[2] C. Koen,[1] D. H. Morgan,[3] J. Barrow,[3] D. A. H. Buckley,[1] R. D. Cannon,[4] C. J. P. Cass,[4] M. R. Cranston,[3] M. Drinkwater,[4] M. Hartley,[4] M. R. S. Hawkins,[3] S. Hughes,[5] C. M. Humphries,[3] H. T. MacGillivray,[3] P. B. McKenzie,[4] Q. A. Parker,[4] M. Read,[3] K. S. Russell,[4] A. Savage,[4] E. B. Thomson,[3] S. B. Tritton,[3] J. D. Waldron,[3] B. Warner[2] and F. G. Watson[5]

[1]*South African Astronomical Observatory, PO Box 9, Observatory 7935, Cape, South Africa*
[2]*Department of Astronomy, University of Cape Town, Rondebosch 7700, Cape, South Africa*
[3]*Royal Observatory, Blackford Hill, Edinburgh EH9 3HJ*
[4]*Anglo-Australian Observatory, PO Box 296, Epping, NSW 2121, Australia*
[5]*Royal Greenwich Observatory, Madingley Road, Cambridge CB3 0EZ*

Accepted 1997 January 10. Received 1996 December 31; in original form 1996 March 20

ABSTRACT

The Edinburgh–Cape Blue Object Survey is a major survey to discover blue stellar objects brighter than $B \sim 18$ in the southern sky. It is planned to cover an area of sky of 10 000 deg^2 with $|b| > 30°$ and $\delta < 0°$. The blue stellar objects are selected by automatic techniques from U and B pairs of UK Schmidt Telescope plates scanned with the COSMOS measuring machine. Follow-up photometry and spectroscopy are being obtained with the SAAO telescopes to classify objects brighter than $B = 16.5$. This paper describes the survey, the techniques used to extract the blue stellar objects, the photometric methods and accuracy, the spectroscopic classification, and the limits and completeness of the survey.

Key words: surveys – stars: early-type – stars: horizontal branch – subdwarfs – white dwarfs – quasars: general.

1 INTRODUCTION

The Palomar–Green (PG) Survey (Green, Schmidt & Liebert 1986) carried out in the 1970s was a major impetus, leading to many new discoveries connected with hot ultraviolet-excess stars. This led directly to a north–south imbalance in the numbers of such objects known. Many of the classes of objects are intrinsically of great interest, and in some cases sufficiently rare that only a few are known. With these thoughts in mind, it was expected that an extension of the PG Survey to the southern hemisphere would yield equally rich returns.

The southern survey was initially proposed by Warner and Cannon in 1984 as an objective-prism survey to be carried out using the facilities of the UK Schmidt Telescope in Australia and the COSMOS measuring machine in Edinburgh. Each objective-prism plate, however, has a limited dynamic range over which it is possible to carry out spectral classification and, consequently, multiple plates of differing exposure are required if one wishes to extend the dynamic range. Because direct plates have a much greater useful dynamic range and are easier to measure automatically, it was decided subsequently to use pairs of direct U and B plates of each field. In 1984 a pilot study was carried out with objective-prism and direct plates of the same fields to determine the optimum strategy. In the limited magnitude range where the objective-prism plates were usable it was clear that the blue stellar objects could be detected reliably from U and B plate pairs. The results showed that with direct plates it would be possible to extract blue stellar objects over a range of at least 8 mag. The full photographic survey commenced in 1985.

The primary aim is to obtain a complete catalogue of blue ($U-B < -0.4$) stellar objects brighter than $B \sim 18$ for fields in the southern celestial hemisphere with galactic latitude $|b| > 30°$. Follow-up photometry and spectroscopy of candidate blue objects at the South African Astronomical Observatory (SAAO) are essential for classification pur-

poses. Although the photometry and spectroscopy are complete only to $B=16.5$, the original survey extracted blue stellar objects to $B\sim18$ as the information was on the photographic plates and it was very little extra effort to select these objects as well.

The Montreal–Cambridge–Tololo Survey of southern subluminous blue stars (Demers et al. 1986) has similar aims in terms of detecting stars brighter than $B=16.5$. This survey uses the combination of double-exposure U/B photographic plates taken with the CTIO Curtis Schmidt Telescope, which are subsequently digitized with the Automated Plate Measuring facility at Cambridge. We expect that many of the extreme blue stellar objects discovered in both surveys will be the same, although there are likely to be differences in the colour selection at the red boundary and in the magnitude selection at the faint end.

The primary categories of object which we expect to discover in this survey are O and B subdwarfs, white dwarfs, blue horizontal branch stars, apparently normal B stars, cataclysmic variables, and bright quasi-stellar objects. In addition, it is of great interest to discover rare objects such as pulsating degenerate stars, magnetic white dwarfs and possibly even new kinds of stellar object. It is important for this reason that all objects be followed up to identify the type, and particularly to place most effort on the so far unclassified objects as it is amongst these that the new discoveries will be made.

This paper describes the overall Edinburgh–Cape Survey, referred to hereafter as the EC Survey, the techniques using in detecting the blue stellar objects and the follow-up photometry and spectroscopy. The survey itself will be published as a series of papers each cataloguing a celestial zone in the survey with photometry and spectroscopy of objects complete to $B=16.5$. The survey has already been briefly described in two papers (Stobie et al. 1988, 1992) and initial results on individual stars, white dwarfs and QSOs have been presented in a number of papers (Kilkenny, O'Donoghue & Stobie 1991; Buckley et al. 1992; Chen et al. 1993; Stobie et al. 1993, 1995; Savage et al. 1993; O'Donoghue et al. 1993, 1994; Kilkenny et al. 1995; Koen et al. 1995).

2 BLUE OBJECT SELECTION

2.1 Plate material

The photographic plates are being taken with the 1.2-m UK Schmidt Telescope (UKST) in Australia, originally operated by the Royal Observatory, Edinburgh (ROE) and now part of the Anglo-Australian Observatory (AAO). The UKST cannot take multiple exposures through different filters, since the filters are incorporated in the plateholders. Consequently, for each field two separate plates are being taken in order to select blue stellar objects. As with the PG Survey, U and B filters are used since better discrimination for the kinds of object we wish to select is obtained from the $(U-B)$ colour than other colour combinations, such as $(B-V)$. The plates are taken as close together in time as possible, normally on the same night, in order to avoid spurious colours arising from objects variable on time-scales greater than a few days.

The emulsion chosen originally was Kodak type IIa-O, as this did not require hypersensitization to reach the desired magnitude limit and it gave a good approximation to the standard U and B photometric bands. About two-thirds of the EC Survey has been done on IIa-O emulsion. However, production of that emulsion has now been discontinued by Kodak, and it is expected that the survey will be completed on IIIa-J emulsion. This will mean some change in the effective passbands, especially by extending the B band to somewhat longer wavelengths, but this should not affect the selection of the bluest objects significantly. The filters used are UG1 for the U exposure and GG385 for the B exposure. The U exposure at 60 min limits the depth of the survey, ensuring that blue objects as faint as $B=18$ will be detected. The B exposure at 15 min is much deeper than the U exposure, reaching about 20 mag. The deeper B exposure was deliberately chosen so that reliable star/galaxy discrimination could be obtained to $B\sim18$. Furthermore, there was little to be gained by a shorter exposure because of the time required to change plates. In order that the EC Survey did not conflict with the primary surveys of the UKST, it was decided that plates would be taken only in non-survey conditions (i.e., seeing >2 arcsec). In retrospect, this was a fortunate decision because accurate wide-field stellar photometry is more difficult with plates taken in good seeing, assuming that one is not dealing with the crowded-field case. The reason is that in good seeing the image structure varies across a wide-angle photograph, resulting in systematically different magnitudes as measured by COSMOS. Although the polar axis elevation of the UKST is adjusted for every photograph, in order to minimize field rotation due to atmospheric refraction, there is an irreducible residual effect (Wallace & Tritton 1979). Poor seeing blurs these effects and makes uniform stellar photometry across a Schmidt plate easier to achieve.

2.2 COSMOS measurement

Up until 1995 all the plates were digitized at the Royal Observatory, Edinburgh with the COSMOS machine (MacGillivray & Stobie 1984) using the 16-μm increment and the 32-μm spot. The later plates are expected to be measured in the new SuperCOSMOS machine. The plates are physically of size 356×356 mm^2. For reasons of mechanical limitations the maximum area that COSMOS could measure was 287×287 mm^2. This area is not quite central on the plate, but it contains nearly all the unvignetted region of the UKST plate. With a plate scale of 67.12 arcsec mm^{-1}, this corresponds to an area on the sky of 5.35×5.35 deg^2. With plate centres 5° apart, this ensures that there is complete sky coverage and a small degree of overlap.

The COSMOS machine is operated in 'thresholded mapping' mode. In this mode the machine follows the variable sky background and determines a threshold at a fixed percentage level in intensity units above the local sky background. The relative intensity calibration is determined from the 16-step sensitometer spots. The threshold level chosen typically corresponds to a 2.5σ cut above the sky background noise.

COSMOS measures in lanes in the y-direction, each lane being 128 pixel wide. The image analysis software collates pixels belonging to the same object, and calculates a set of parameters based on the image moments up to second

order. Both unit-weighted and intensity-weighted parameters are calculated. The lanes accurately abut each other, and images that are split across lane boundaries are combined later. In recent years the COSMOS image analysis has incorporated image deblending software (Beard, MacGillivray & Thanisch 1990). This was not used for the present project for two reasons: (i) because of the fundamental non-linearity of the photographic process the magnitudes of deblended images are not as accurate as those of isolated images and can contain systematic, although relatively small, errors, and (ii) the image deblending software considerably increases the total analysis time. With the simpler image analysis software, the total measuring plus analysis time per plate was 5 h. Because the EC Survey is limited to fields with $|b| > 30°$, the stellar density was never so high that this lack of image deblending was a problem. A small fraction of blue stellar objects that are blended will have been missed as a result. In the detection process any candidate blue objects which turned out to be merged images were excluded at the visual inspection stage. Because the image analysis applied only to isolated stellar objects, any merged object was excluded as the photographic photometry was not reliable.

2.3 Image parameters

COSMOS outputs a catalogue of detected objects with a set of parameters describing each object. Most of these parameters were not necessary for the present project. To save on subsequent storage requirements, only a minimum set was retained, consisting of

B plate: RA, Dec., area, COSMAG, I_{sky}, a, b, θ, x, y,
U plate: RA, Dec., area, COSMAG, I_{sky}, a, b, θ.

The RA and Dec. are produced by COSMOS software by automatically pairing with existing astrometric catalogues, given the RA, Dec. of the plate centre, the plate scale and the plate orientation during measurement. These coordinates are accurate to 1 arcsec, and are required for both the pairing of the plates and the production of computer finding charts. The area is the number of pixels in the image. An area cut of 10 pixel was normally applied to avoid storage of images below this size. These images are in any case very faint (typically $B > 20$) and of too low photometric accuracy for this project. The COSMAG parameter is defined as $-250 \log \sum_i (I_i - I_{sky})$, where the summation is over all pixels in the image, and the intensities are relative intensities obtained from the step-wedge calibration. The semimajor axis, the semiminor axis and orientation (a, b, θ) are obtained from fitting an ellipse to the second-order, unit-weighted moments (Stobie 1986) and were primarily used for the identification of elliptical images (usually galaxies or doubles). The x,y centroids were retained to produce an x,y plot at the scale of the Schmidt plate to aid in the visual inspection.

2.4 Plate pairing

The same object on each plate had to be paired to produce a merged catalogue. The parameters RA and Dec. on the *U* and *B* plates were used for this. The *B* plate was taken as the primary catalogue, and the images on the *U* plate were paired, using a hash table, if they fell within a square box of size ± 3 arcsec of an image on the *B* plate. Different error box sizes were experimented with, and it was found that ± 3 arcsec was close to optimum. More pairing takes place as the error box size increases, but too large an error box will produce spurious pairings. If the error box is reduced below about 2 arcsec, then on some plate pairs there will be large numbers of images not pairing, especially at the edges of the measured area. The reason for this is that the automatic RA, Dec. conversion process has successive 3σ rejection of outliers in the iteration to a plate solution. Sometimes this can lead to systematic errors in the transformation of x,y to RA, Dec. which, although they do not exceed ± 0.5 arcsec, can be sufficient to cause problems with too tight an error box. With an error box of ± 3 arcsec, 96 per cent of the objects on the *U* plate with area > 10 pixel were successfully paired with a corresponding image on the *B* plate. The images which did not pair were either doubles which had merged on one plate but were detected as two separate images on the other plate, or were satellite trails, asteroid trails or some kind of plate flaw.

2.5 Star/galaxy discrimination

Because of non-linear effects in the photographic emulsion and density saturation effects in the COSMOS measuring machine, the stellar and galaxy magnitude calibrations are quite different. It was thus considered safer to exclude the galaxies from the blue object selection, and for this reason star/galaxy discrimination was necessary. Because the *B* plate was deeper, the parameters from this plate provided the star/galaxy discrimination. A number of different techniques were tried, and it was found that the surface brightness criterion in the log(area)–COSMAG plot was the most reliable (Fig. 1). Initially, this plot was used to place a polygon surrounding the stellar objects and to extract only objects whose parameters lay within the polygon. At faint magnitudes where the stellar and galaxian sequences merged this meant that galaxies were classified as stellar but, as this was typically at magnitudes $B > 18$, for $B < 18$ there was very little contamination by galaxies.

This star/galaxy discrimination procedure was subsequently automated by fitting a spline to the mode of the distribution (which is heavily dominated in this magnitude range by the stellar sequence) and defining a line corresponding to a specified sigma cut. The sigma cut was determined for each magnitude bin by defining $X_{max} = X_{mode} + (1 + C)\sigma$, where $X = \log(\text{area})$ and X_{mode} is the modal value, and σ is the standard deviation of the distribution of X values for a given magnitude bin. The value of $C = \sum |X_i - X_{mode}| / N\sigma$ is a parameter that determines the absolute scatter of the distribution relative to its standard deviation. In practice, C varies as a function of magnitude, as the distribution from which it is determined is both non-Gaussian and skew. The objects below the line correspond to images of point sources and were classified stellar. The objects above the line are more extended than point source images and were classified non-stellar. In practice, the star/galaxy discrimination was effective to $B \sim 18$ (COSMAG ~ -1000). Fainter than this it can be seen that the stellar and galaxian objects merge, and there is insuffi-

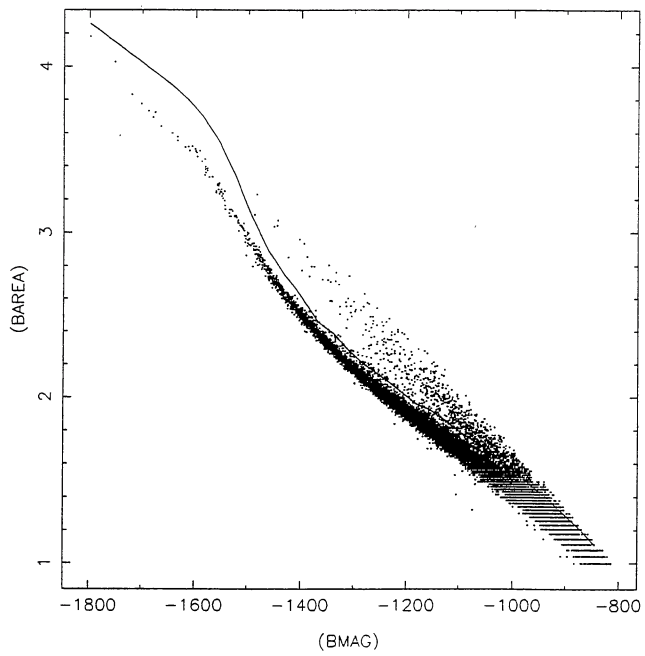

Figure 1. Star/galaxy discrimination using a surface brightness criterion. The ordinate is log(area) where area is the number of pixels in the object. The abscissa is COSMAG which is related to the volume integral of the intensity above sky. The line defines the upper limit to the stellar population (see text).

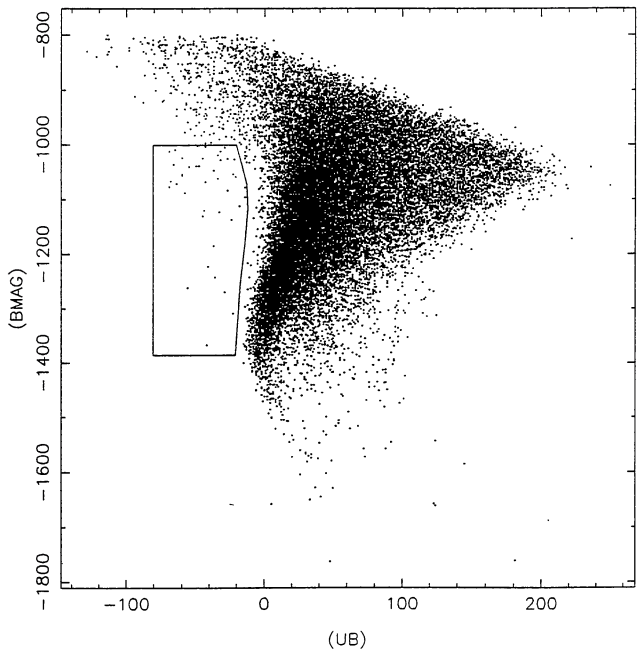

Figure 2. The selection of blue stellar objects in the natural system B, $U-B$ magnitude–colour diagram. The polygon defines the objects of interest down to a faint magnitude limit of $B \sim 18$.

cient information on these plates to distinguish between them.

2.6 Blue object selection

This was carried out in the natural system B, $U-B$ diagram of the stellar objects (Fig. 2). At faint magnitudes the effects of the B-plate limiting magnitude (10-pixel area cut-off) and the U-plate limiting magnitude can be seen. Ideally, these photographic magnitudes should be converted to the Johnson B, $U-B$ magnitude–colour diagram. However, this would require photoelectric and CCD standards in every field and effectively would have doubled the size and timescale of the project. It was clear from preliminary photographic B, $U-B$ diagrams that the interesting blue objects could be readily identified. As these blue objects subsequently were to be observed photometrically and spectroscopically, the survey in practice could be post-calibrated in order to derive a statistically complete sample according to uniform B, $U-B$ selection criteria.

Fig. 2 shows an example of the selection polygon enclosing the interesting blue stellar objects. The selection polygon is determined by eyeball on a field-by-field basis to include the blue stellar objects and exclude as far as possible the F/G-type stars. There is a relatively sharp boundary between the F/G-type stars and the bluer objects. The curvature in the F/G-type locus is caused by the non-linear response of the photographic emulsion and the saturation of the COSMOS measuring machine. This shape varies from field to field. The boundary becomes less sharp at fainter magnitudes, because the photometric errors are increasing. The location of the red edge of the polygon is critical. If it is positioned too red, then too many F/G-type stars will contaminate the blue sample. If it is too blue, then, although the F/G-type contamination will decrease, some of the interesting blue objects may be missed. A level of ~ 20 per cent F/G-type stellar contamination was considered acceptable. The majority of these F/G types were identified from the accurate photoelectric *UBV* photometry, and it was not necessary to observe them spectroscopically. The number density of blue stellar objects selected varied as a function of galactic latitude and longitude with, on average, about 50 objects per field, corresponding to a number density of 2 per square degree.

2.7 Visual inspection

To exclude spurious candidates, all blue objects were inspected visually on both the U and B plates. To aid in this inspection, (1) an xy underlay at the scale of the photographic plate was plotted with all blue objects, together with ~ 30 of the brightest stellar objects for accurate registration of the underlay, and (2) a 10×10 arcmin^2 finding chart from the B plate was produced for each object. This enabled rapid accurate identification of the relevant object on the photographic plate. These computer-generated finding charts were subsequently used at the SAAO telescopes for identification of the correct object for photometry and spectroscopy.

The xy underlay was also useful to check the xy distribution of blue stellar objects. If the xy distribution did not look random, then the plates were inspected carefully to identify the reason. Two situations occurred where the xy distribution was not random. In the first case the proximity of the Large Magellanic Cloud or Small Magellanic Cloud affected the gradient of blue stellar objects across neigh-

bouring fields. These were accepted as genuine blue stellar objects, and none was excluded. The second case arose from problems with the focus on the plates. In a few *xy* plots there was a concentration of blue stellar objects to a corner or small region of the plate. The reason was usually that this region of the *U* plate was out-of-focus compared to the rest of the *U* plate. The effect that this has is an increased COSMOS *U* magnitude, because the image, being more out-of-focus, is less saturated and COSMOS measures an increased volume integral of intensity. For example, one factor that caused this in three successive *U* plates was that the *U* plateholder had accidentally a small piece of glass on one edge. With the fast focal ratio of the Schmidt telescope the images in this region were significantly out-of-focus. If such a problem occurred, and it affected only a small fraction of the plates, the solution was to exclude this *xy* region from the blue object selection.

One parameter that was useful to exclude spurious blue objects was the ratio of minor to major axes (b/a) of the ellipse fitted to the second-order moments of the image pixel distribution. Normally an isolated stellar image will have $b/a > 0.7$. If $b/a < 0.7$, the image was examined carefully and usually rejected. If the image was a multiple stellar image, it was rejected as the photometry was not reliable. Other reasons for rejection were if the stellar image on the *U* plate intersected a satellite trail, an asteroid trail or emulsion flaw, thus causing a spuriously bright *U* magnitude.

All cases of rejection were where a problem had occurred on the *U* plate which caused a spuriously bright *U* magnitude. Presumably a very small percentage of genuine blue stellar objects were lost, because a corresponding problem on the *B* plate would cause a spuriously bright *B* magnitude and thus a genuine blue object could appear red.

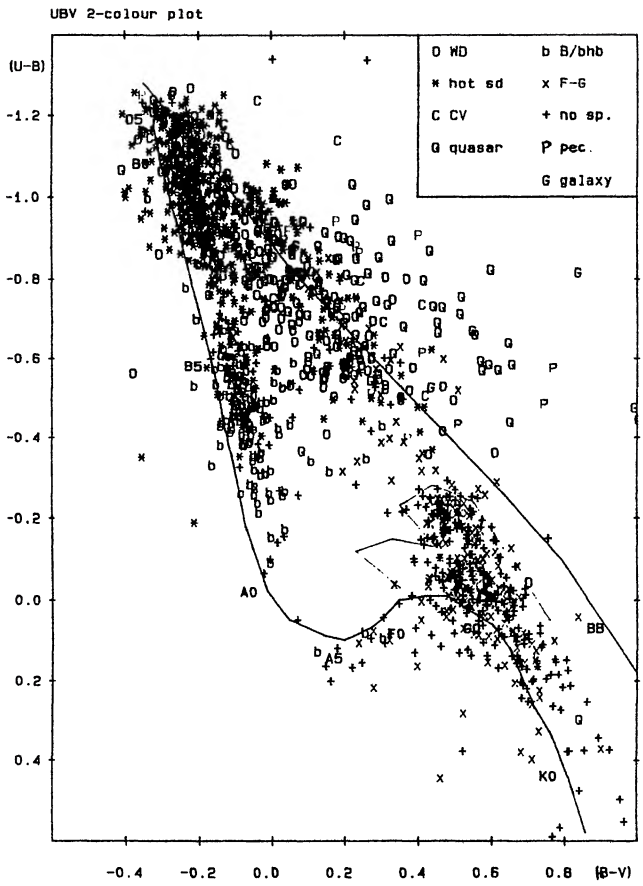

Figure 3. The $(U-B, B-V)$ two-colour diagram for candidate blue objects, the majority of which have spectroscopic classifications. The intrinsic colour line for the main-sequence stars and the blackbody line are shown.

3 PHOTOMETRY

3.1 Photoelectric photometry

UBV photometry is being obtained for all candidate blue stellar objects brighter than $B = 16.5$. The photometry is carried out with either the University of Cape Town photometer on the 0.75-m telescope or the St Andrews photometer on the 1.0-m telescope at the Sutherland outstation of the SAAO.

All data are transformed to the Cousins E-region system using observations of several *UBVRI* standard stars on each night (see Menzies et al. 1989 for the most recent compilation of E-region standard star photometry). A minor problem with these (and other) standards is a lack of extremely blue objects; most E-region standards are redder than $U-B = -0.7$, and the few bluer standards are typically too bright to observe with the Sutherland equipment. On the other hand, most of the survey stars are bluer than $U-B = -0.7$ (see Fig. 3), and we have therefore observed a number of very blue stars from the Menzies, Marang & Westerhuys (1990) compilation (MMW) and forced the blue end of our transformations to fit these stars. The photometry is a continuing process, but we list in Table 1 the current results for these very blue stars, together with their standard deviations. The difference between the photometry of Menzies et al. (1990) and our photometry has mean values (MMW – EC) and standard deviations:

Table 1. *UBV* photometry of Menzies, Marang & Westerhuys (1990) stars.

Star	V	(B-V)	(U-B)	n	σ_V	σ_{B-V}	σ_{U-B}
HD 4539	10.277	-0.235	-0.876	2	0.010	0.006	0.007
HD 18100	8.474	-0.235	-0.947	14	0.009	0.007	0.003
HD 29557*	8.612	-0.140	-0.445	14	0.029	0.011	0.037
HD 49798	8.284	-0.284	-1.158	18	0.008	0.006	0.006
HD 61943	7.797	-0.158	-0.654	4	0.011	0.008	0.004
HD 63169	9.805	-0.128	-0.757	3	0.013	0.004	0.003
HD 76431	9.228	-0.280	-1.034	8	0.015	0.004	0.005
UVO 0832-01	11.438	-0.287	-1.198	1			
UVO 0904-02	11.942	-0.303	-1.205	6	0.006	0.007	0.002
HD 90786	8.806	-0.051	-0.756	3	0.007	0.002	0.003
HD 115770	8.528	-0.112	-0.586	10	0.005	0.004	0.006
UVO 1419-09	12.090	-0.290	-1.156	19	0.009	0.006	0.013
HD 146463	8.110	-0.051	-0.635	2	0.001	0.006	0.005
HD 149382	8.941	-0.279	-1.085	7	0.007	0.002	0.008
HD 161791	8.456	-0.019	-0.512	4	0.014	0.010	0.011
HD 171858	9.842	-0.216	-0.955	6	0.007	0.006	0.011
HD 188112	10.186	-0.180	-0.803	11	0.006	0.007	0.006
HD 205805	10.181	-0.237	-0.930	15	0.006	0.004	0.005
HD 217507	9.143	-0.209	-0.829	9	0.005	0.002	0.006

*Probable variable.

$\Delta V = 0.000 \pm 0.014$,

$\Delta(B-V) = -0.001 \pm 0.005$,

$\Delta(U-B) = +0.002 \pm 0.008$

from 17 stars (excluding the probable variable HD 29557), and there are no significant colour effects in the range $-0.5 > U-B > -1.2$. It appears that our *UBV* photometry of survey stars should be close to that of Menzies et al. (1990) (the overlap stars are a mixture of normal B stars and hot subdwarfs), and the small internal errors in Table 1, on average <0.01 mag in all quantities, suggest that we have maintained good internal consistency over several years with two telescopes and two photometers.

Of course, the Table 1 stars are all relatively bright, so the internal errors are not representative of the survey as a whole. As most objects were observed only once, it is not easy to estimate the errors in the survey photoelectric photometry. Where objects were observed more than once, it was usually because the object was suspected to be variable or that the first observation was obtained in slightly suspect conditions. These data are not ideal for estimating the internal errors of the survey photometry, but we have attempted to do this, eliminating obvious variables and clearly poor data. The mean standard deviations are listed in Table 2 as a function of magnitude range but, for the reasons noted above, should be regarded as indicative rather than precise values.

Table 2. Standard deviations for EC Survey stars.

magnitude	σ_V	σ_{B-V}	σ_{U-B}	n_{obs}	n_*
$V < 13.5$	±0.01	±0.01	±0.02	55	24
$13.5 < V < 14.5$	±0.02	±0.01	±0.02	34	13
$14.5 < V < 15.5$	±0.02	±0.02	±0.02	42	20
$15.5 < V < 16.5$	±0.02	±0.04	±0.02	34	17
$16.5 < V$	±0.04	±0.04	±0.05	17	8

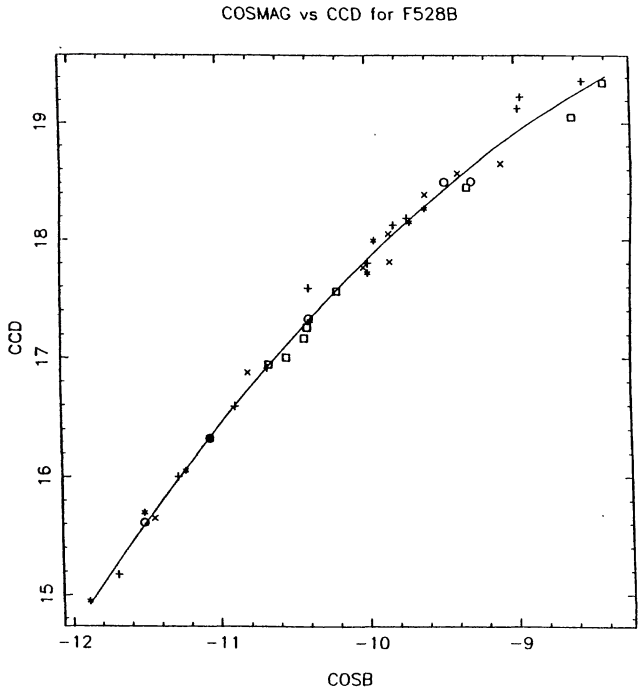

Figure 4. Magnitude calibration of a 15-min exposure *B* plate with CCD observations. The different symbols correspond to five different CCD frames over the area of the Schmidt plate.

The $(U-B, B-V)$ two-colour diagram for a sample of stars in the survey is shown in Fig. 3. The spectroscopic classification is described in Section 4. The two-colour diagram clearly identifies a number of subgroups. The F/G-type subdwarfs fall within a boundary stretching from the Hyades main sequence to an upper locus defined by the most metal-poor subdwarfs. One of the uses of the photometry is that any star falling within this domain is classed as an F/G subdwarf, and usually no further photometry or spectroscopy of it is obtained. Another group of stars are the blue horizontal branch stars and normal B stars. By far the most common types of object (accounting for ~50 per cent of the survey) are the O and B subdwarfs. These stars cover a wide range of temperatures, which are so high that the *UBV* photometric system provides no discrimination in temperature. Spectroscopy is essential to distinguish the different types of O/B subdwarf with differing temperatures, gravities and chemical abundances. The remaining objects tend to cluster around or above the blackbody line, and are a diverse group comprising white dwarfs, cataclysmic variables, QSOs and compact emission-line galaxies.

The faint magnitude cut-off in the selection of blue stellar objects was typically chosen as COSMAG = −1000. It can be seen from Fig. 4, which shows the magnitude calibration of COSMAG values versus the CCD calibration in a representative field, that this corresponds to $B \sim 18.0$. A further check on this magnitude calibration can be obtained approximately from the Bahcall & Soneira (1980) galaxy model, giving star counts in *B* as a function of galactic latitude and longitude. This model was determined for every field based on the position of the plate centre and the area of sky measured, namely 28.6 deg^2. The fields all showed that the magnitude cut-off of COSMAG = −1000 corresponded to a *B* magnitude cut-off in the range $17.5 < B < 18.5$.

3.2 Accuracy of the *U* and *B* photographic photometry

The completeness of the catalogue of ultraviolet-bright stars depends critically on the accuracy of the photographic $U-B$ colour measurement. Investigation of this is possible using the *UBV* photoelectric photometry with which the photographic photometry can be calibrated. Previous experience with wide-angle Schmidt photographs and automated measuring machines would lead one to expect errors in *U*, *B* photographic magnitudes of ~0.1 mag for isolated stellar images more than 2 mag above the plate limit (Reid & Gilmore 1982; Stobie & Ishida 1987). This leads to an expected accuracy of ~0.15 mag for the photographic $(U-B)$ colour.

O'Donoghue et al. (1993) have assessed the accuracy of the photographic photometry in the EC Survey on the basis of almost 90 fields for which photoelectric photometry is complete to $B \sim 16.5$. For each of these fields, plots of photographic photometry (hereafter called Cos *U* and Cos *B*) versus photoelectric photometry (called U_{pe} and B_{pe} respectively) were produced. For some fields, tight parabolic relationships between Cos *U* and U_{pe}, and Cos *B* and B_{pe} were

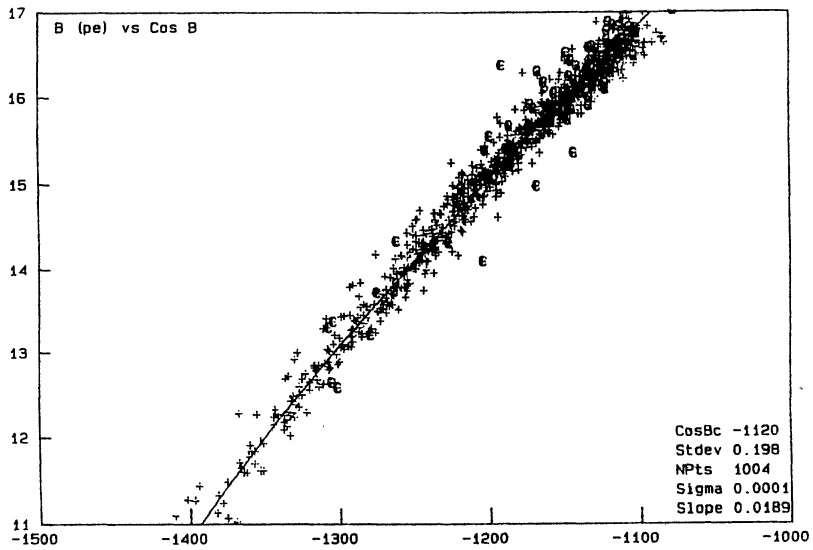

Figure 5. Combined plot of B_{pe} (ordinate) versus Cos B (abscissa).

found, with residual standard deviations of ~ 0.1 mag. For the majority of fields, however, the residual scatter was much worse: 0.2 mag typically, but occasionally reaching as large as 0.3–0.4 mag. This result would seem to imply that Cos $U-B$ is measured with an accuracy of 0.3 mag or worse!

For most fields the number of stars that could be used in the calibration was less than 15; additionally (known) variables amongst the blue objects had to be excluded. In order to gain an overall assessment of the accuracy of the photographic photometry, the results for all the completed fields were combined. This necessitated determining the arbitrary zero-point for each field by fitting a parabola with fixed linear and quadratic coefficients to the plots of Cos B versus B_{pe} (and Cos U versus U_{pe}). This zero-point was then subtracted from all the stars within the corresponding field, allowing a single plot of Cos B versus B_{pe} (Fig. 5) or Cos U versus U_{pe} to be made. The scatter in the residuals about the best-fitting parabola was found to be 0.20 mag for Cos B and 0.30 mag for Cos U, with most of the additional scatter in Cos U coming from sdF and sdG stars with $U-B > -0.2$. This additional scatter is not random: the residuals of the sdF and sdG stars are systematically biased towards brighter values of Cos U than implied by their values of U_{pe}.

The presence of these sdF and sdG stars is clearly seen in the $(U-B, B-V)$ two-colour diagram for a sample of stars in the survey with photoelectric photometry (Fig. 3). It is apparent in this diagram that there is a dearth of horizontal branch A stars ($B-V_{pe}=U-B_{pe}=\sim 0.0$), but significant contamination (~ 20 per cent) of the survey sample by sdF and sdG stars ($U-B_{pe} \geq -0.2$, $B-V_{pe} \geq 0.4$). Taken at face value, this seems to imply that there is a strong colour term in the relation between Cos $U-B$ and $U-B_{pe}$, which results in objects which are redder in $B-V$ being selected at redder $U-B_{pe}$.

Considerable effort was expended in trying to find a colour term in the relationship between Cos U and U_{pe} which would account for the contamination of the survey sample by red subdwarfs. However, plots of the residuals versus colour in the Cos U and U_{pe} relation yielded no consistent colour term. This failure to find a colour term agrees with the colour equations derived by Blair & Gilmore (1982) for the combination of UKST, filters and IIa-O emulsion used in the EC Survey.

3.3 Non-Gaussian errors in the photographic photometry

It has long been recognized that the error distribution in photographic photometry is non-Gaussian (Gilmore 1983) and shows an extended tail. This is an important effect if one is carrying out a photographic survey for objects of extreme colour or unusual properties, such as variables, as the non-Gaussian tail leads to a small fraction of 'normal' stars contaminating the desired sample with spurious candidates.

To estimate the importance of this effect for the EC Survey, the non-Gaussian error distribution was assumed to be the same as that based on a seven-plate merge of UKST V plates taken of the South Galactic Cap (Stobie & Henley 1983). These data define the plate-to-plate errors in terms of rms(COSMAG) units for different magnitude ranges. These numbers were converted to photoelectric magnitudes using standards and CCD sequences in the South Galactic Pole region. The number of normal sdF and sdG stars predicted to be scattered into the blue object selection by these non-Gaussian errors was estimated by taking the distribution of $(U-B)$ colours for the magnitude range $V<18$ as derived for the North Galactic Cap (Yoshii, Ishida & Stobie 1987). It was found for $13.2<V<15.0$ that 1 per cent of the stellar images had rms >0.15 mag, and 0.5 per cent had rms >0.21 mag. For $16.5<V<17.0$ it was found that 4 per cent of the stellar images had rms >0.15 mag and 0.7 per cent had rms >0.21 mag. Thus stars with intrinsic $(U-B)$ in the range $-0.2<(U-B)<0.0$, which would not normally be selected as ultraviolet-rich stars, can be scattered into the ultraviolet-rich region of $(U-B)<-0.4$. Because the F/G stars so outnumber the intrinsically blue stars, even a small percentage of non-Gaussian errors can cause significant contamination. Detailed calculations have shown that the

observed ~20 per cent contamination of F/G stars in the survey can be explained entirely by the non-Gaussian error distribution.

This result also explains why the sdF and sdG stars appear to affect only the Cos U photometry: those objects showing anomalously bright Cos B values would not be selected by the survey technique.

3.4 Accuracy of $U-B$ photographic colour and correlated errors

With the recognition that the sdF and sdG stars, which were photographically selected as apparently blue stellar objects, have anomalously large errors in the photographic photometry, it was clear that the calculations of Section 3.2 had to be repeated after excluding all objects with $U-B_{pe} \geq -0.3$. The result for the B mag calibration is similar to that obtained before, with the standard deviation of residuals, 0.20 mag, showing only a slight improvement by the exclusion of the red subdwarfs. The U mag calibration showed a similar plot to the B mag calibration, but now with a much smaller scatter, 0.22 mag, in comparison to the previous value of 0.30 mag when the red subdwarfs were not excluded.

The most interesting relationship is between Cos $U-B$ and $U-B_{pe}$, which is shown in Fig. 6. The standard deviation of the residuals about the best linear fit shown is only 0.16 mag, smaller than the errors on Cos U or Cos B, and much smaller than the value of 0.30 mag obtained by adding the errors in quadrature. The reason for the smaller error in Cos $U-B$ is simply that the residuals in Cos U and Cos B are correlated. This is clearly illustrated in Fig. 7, which shows a plot of the residuals of the B_{pe} versus Cos B (Fig. 5) against those of the U_{pe} versus Cos U relation.

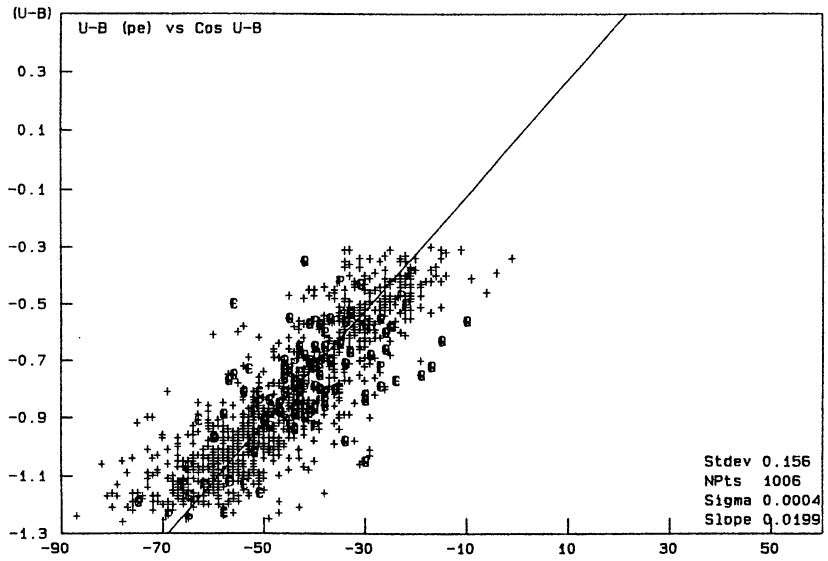

Figure 6. Combined plot of $(U-B)_{pe}$ (ordinate) versus Cos $U-B$ (abscissa).

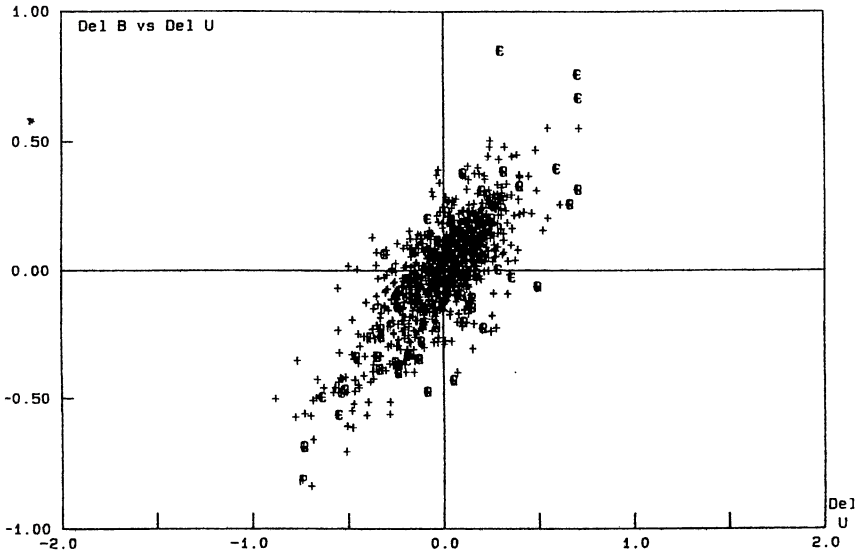

Figure 7. Correlation of residuals in Cos B (ordinate) versus residuals in Cos U (abscissa).

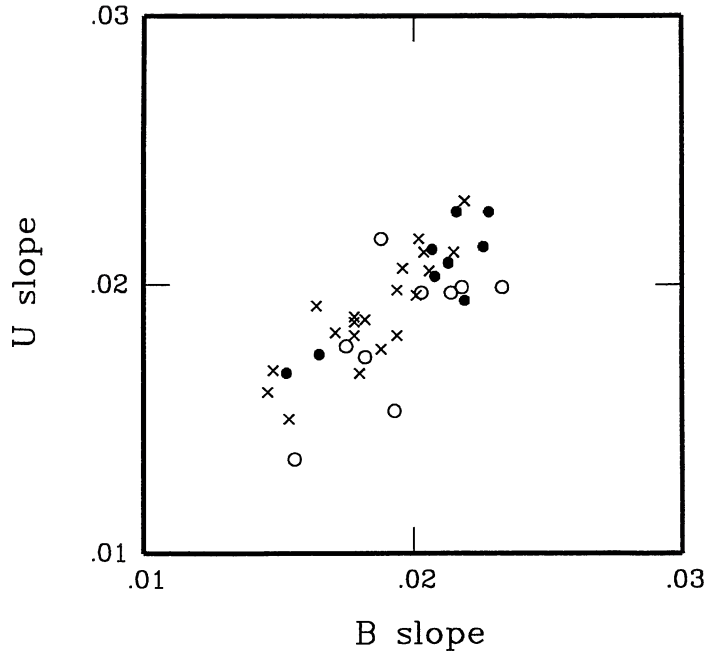

Figure 8. Correlation of magnitude slope of U plate (excluding F/G-type stars) with magnitude slope of B plate for same field. The different symbols reflect how well determined the U and B magnitude slopes are from good (crosses), moderate (filled circles) to poor (open circles).

The strong correlation of the errors in Fig. 7 is obviously intimately associated with the cause of the disturbingly large scatter in the B_{pe} versus Cos B and U_{pe} versus Cos U relations. In this connection, it is important to remember that the U and B photography is done on different plates (normally from the same emulsion batch) but as close together in time as possible. One effect which could cause such a correlation is if the slopes of the B_{pe} versus Cos B and U_{pe} versus Cos U relations differed from field to field but were correlated in the sense that if the slope of the B-magnitude relation is higher than the mean, then so also is the slope of the U-magnitude relation. To test this explanation, the slope of the U-magnitude relation (excluding the F/G-type stars) based on the photoelectric measures for an individual field was plotted against the slope of the B-magnitude relation for the same field (Fig. 8). Fig. 8 clearly shows that these two slopes are highly correlated. The reason for this correlation is probably because the characteristic curve varies from emulsion batch to emulsion batch and as a function of the plate processing, and since both B and U plates were normally taken from the same emulsion batch and often processed together, this causes the correlation of the slopes. Thus the principal reason for the correlation of the residuals between the U and B plates is the correlation in the slopes of the magnitude relations of the plates of the same field. Although this explanation is the principal reason for the correlated residuals, it should be noted that within a given field there is evidence for further correlation of magnitude residuals between the B and U plates. This further correlation is not a function of position on the plate. Strenuous attempts have been made to identify the remaining cause of these correlations, so far without success.

The empirical result of this investigation is that blue stellar objects in the EC Survey are being selected with an accuracy in photographic $U-B$ of 0.16 mag (1σ). This result compares very favourably with the corresponding value of 0.38 mag for the PG Survey (Green et al. 1986). The individual photographic magnitudes, however, are being measured with lower accuracy ($\sim$0.20 mag) than the $(U-B)$ colours.

4 SPECTROSCOPY

4.1 Spectrograph + RPCS system

A spectrogram is being obtained for every object brighter than $B=16.5$ for which the UBV photometry, if obtained first, did not place the object in the F/G subdwarf region of the two-colour diagram. Each spectrogram is obtained with the grating spectrograph and intensified Reticon photon counting system on the SAAO 1.9-m telescope. Grating 6, giving a reciprocal dispersion of 100 Å mm^{-1} and blazed to be optimum at 4300 Å, is used for all spectroscopy. With a normal slit width of 250 μm, corresponding to 1.8 arcsec, the effective resolution is $\sim$3.5 Å. The spectral range covered is $3400<\lambda<5400$ Å, although, because of the fall-off in the intensification chain at the edges, the useful wavelength range is limited to $3600<\lambda<5200$ Å.

The spectrograms are obtained by observing the object in one of the two Reticon arrays and the sky in the other. The object and the sky are then switched between the two arrays and the observation repeated. The object is then observed in the other array. All observations are preceded and followed by Cu/Ar arc spectra to achieve wavelength calibration. For long exposures, an arc is observed in the middle of the sequence. The overall stability is found to be better than 0.3 Å during each night.

The data are sky-subtracted and corrected for pixel-to-pixel variation using flat-field exposures obtained at the start and end of each night. Conversion from counts to flux

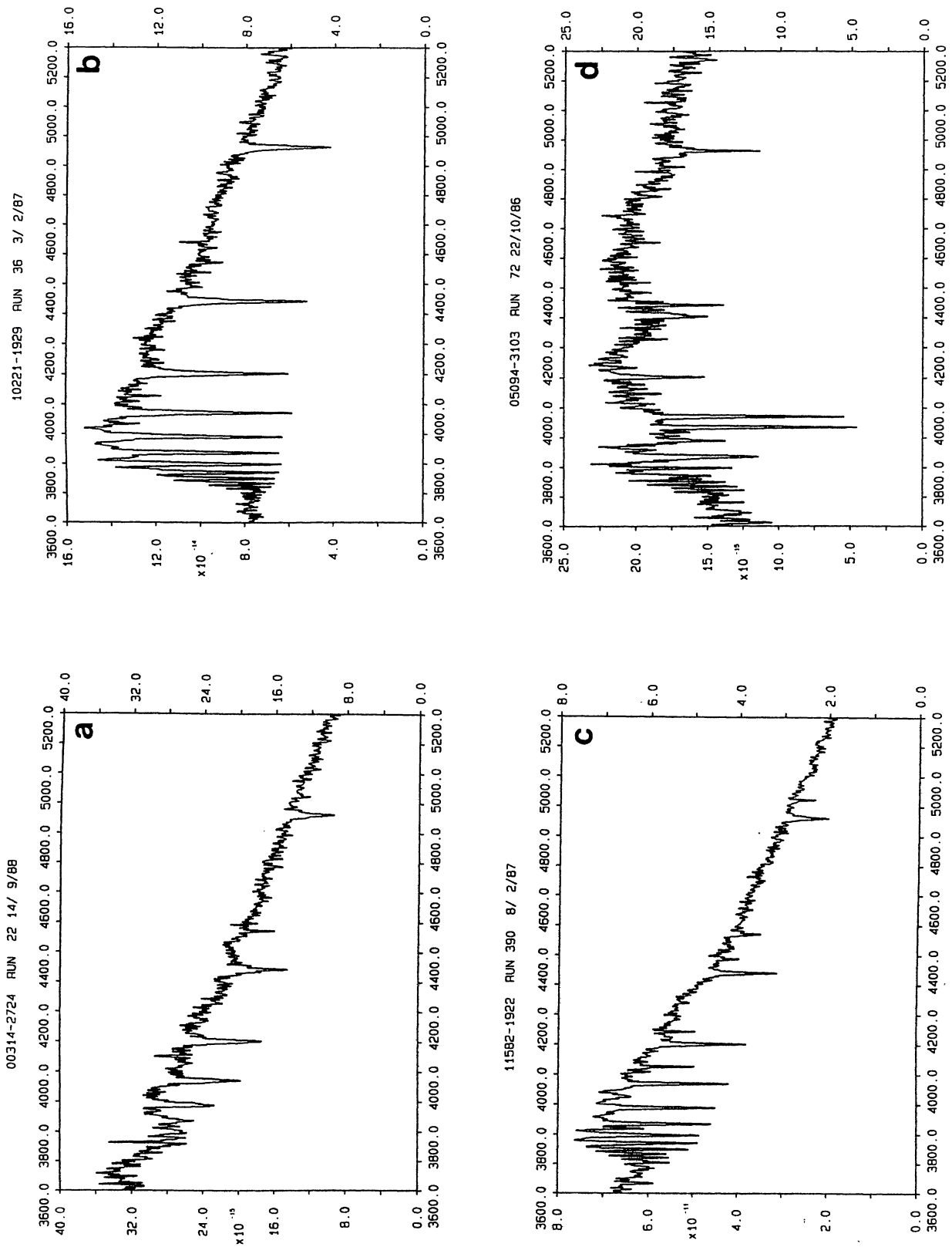

Figure 9. Spectrograms of four early-type stars. (a) Subdwarf B type, (b) blue horizontal branch star, (c) early B type, (d) F/G type.

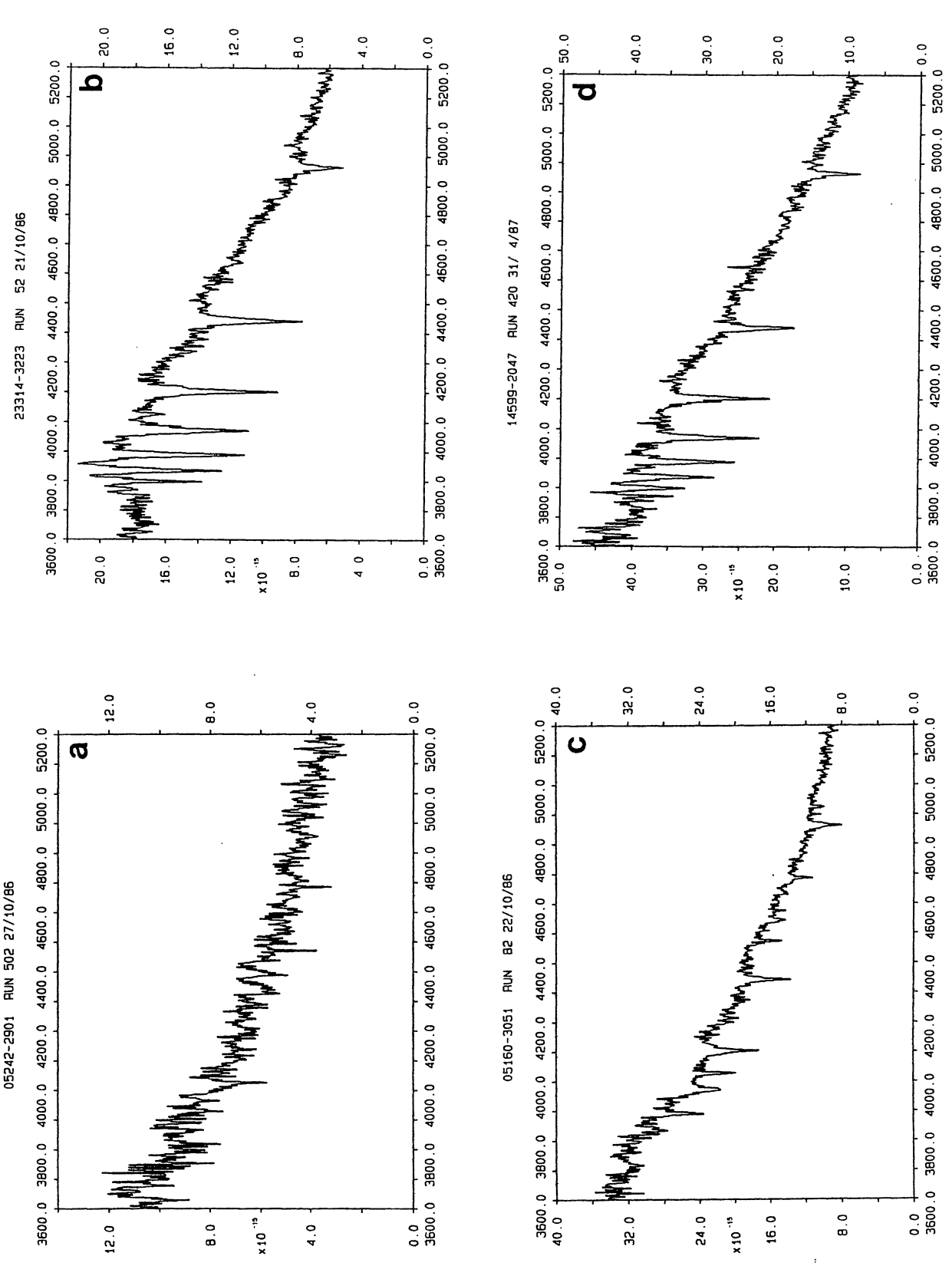

Figure 10. Spectrograms of hot subdwarf stars, all with similar $(U-B, B-V)$ colours. (a) He-sdO, (b) sdOB, (c) sdO, (d) sdB.

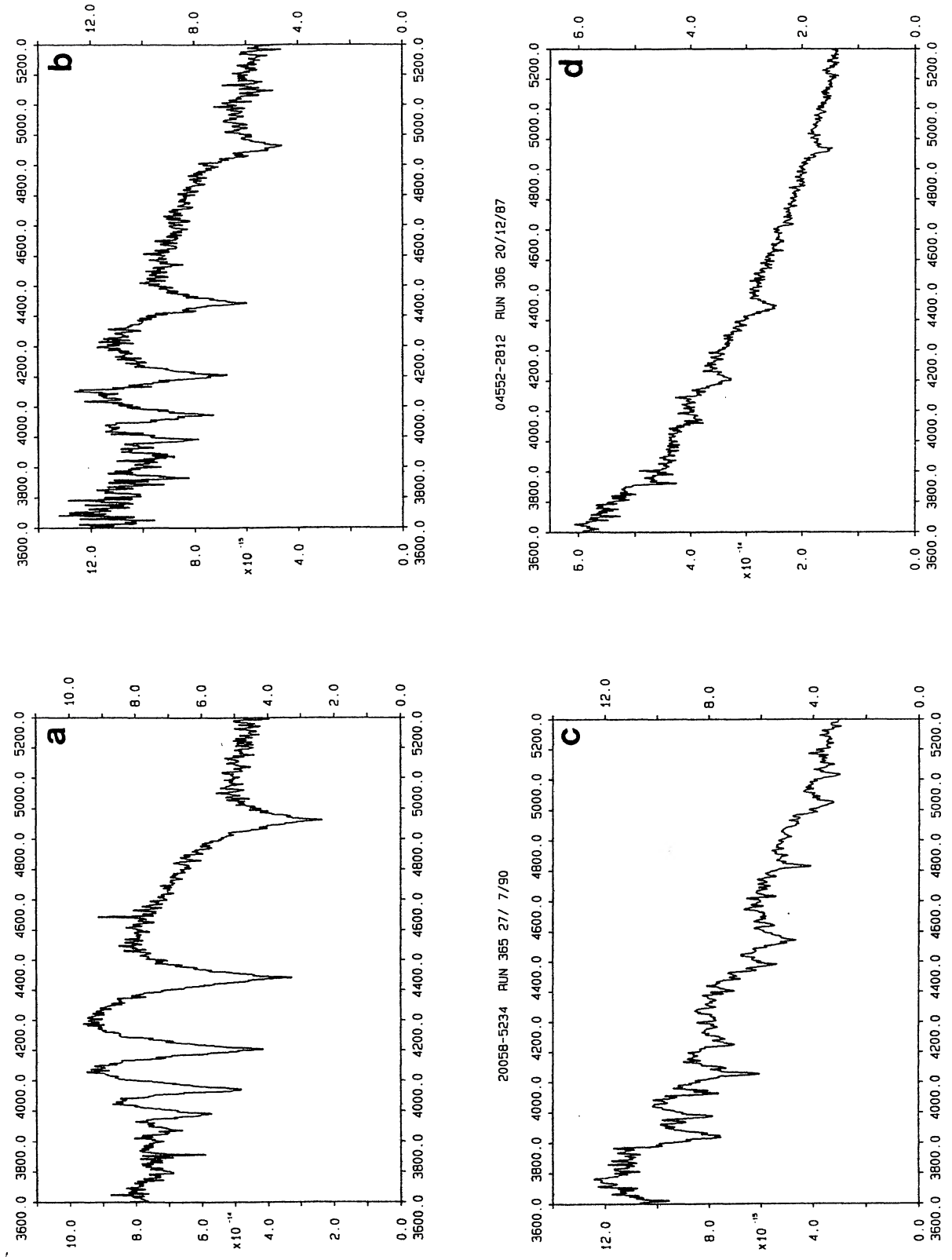

Figure 11. Spectrograms of four white dwarfs. (a) DA, (b) DA with strong hydrogen and weak helium, (c) DB, (d) DA with weak hydrogen.

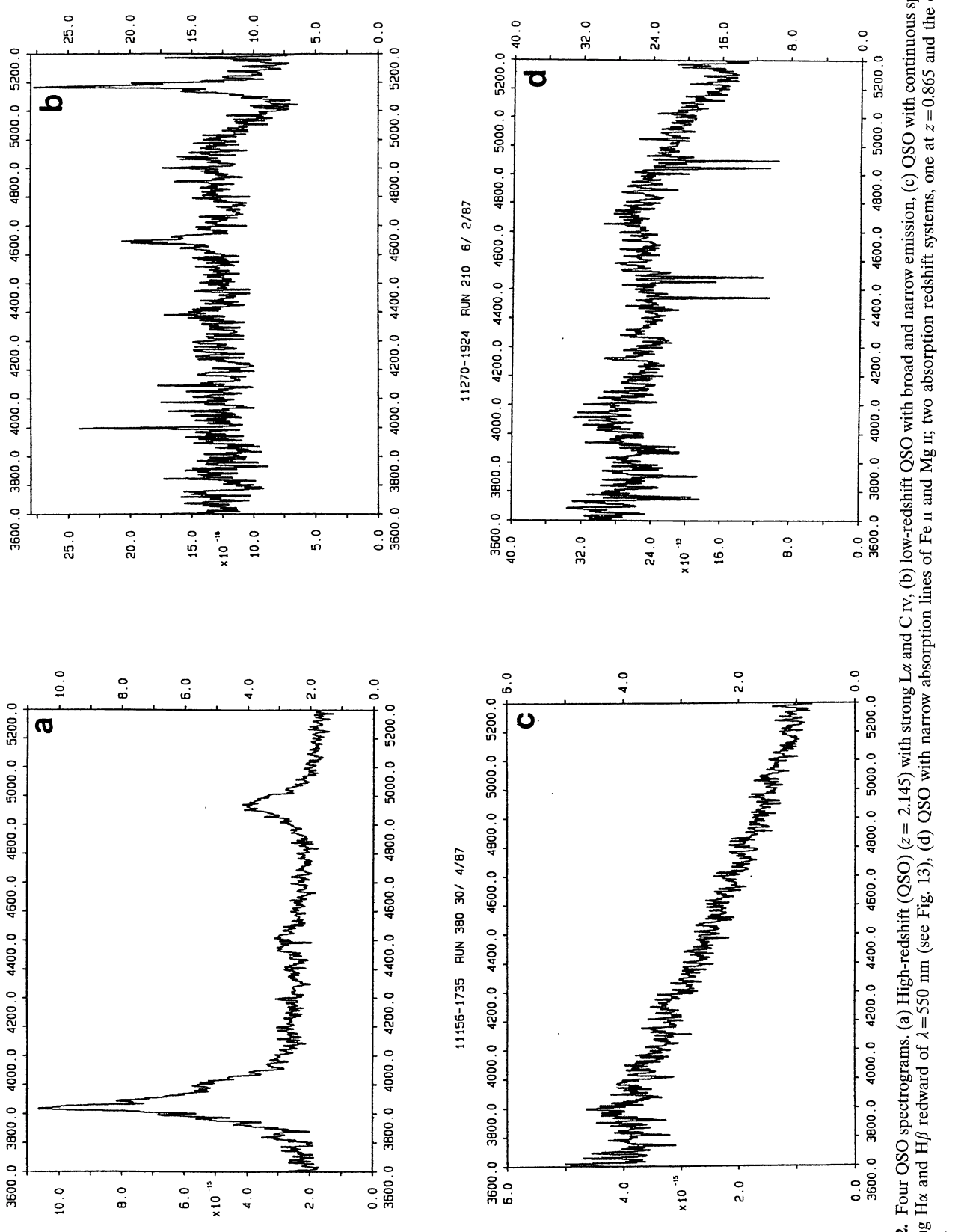

Figure 12. Four QSO spectrograms. (a) High-redshift (QSO) ($z = 2.145$) with strong Lα and C IV, (b) low-redshift QSO with broad and narrow emission, (c) QSO with continuous spectrum but strong Hα and Hβ redward of $\lambda = 550$ nm (see Fig. 13), (d) QSO with narrow absorption lines of Fe II and Mg II; two absorption redshift systems, one at $z = 0.865$ and the other at $z = 0.314$.

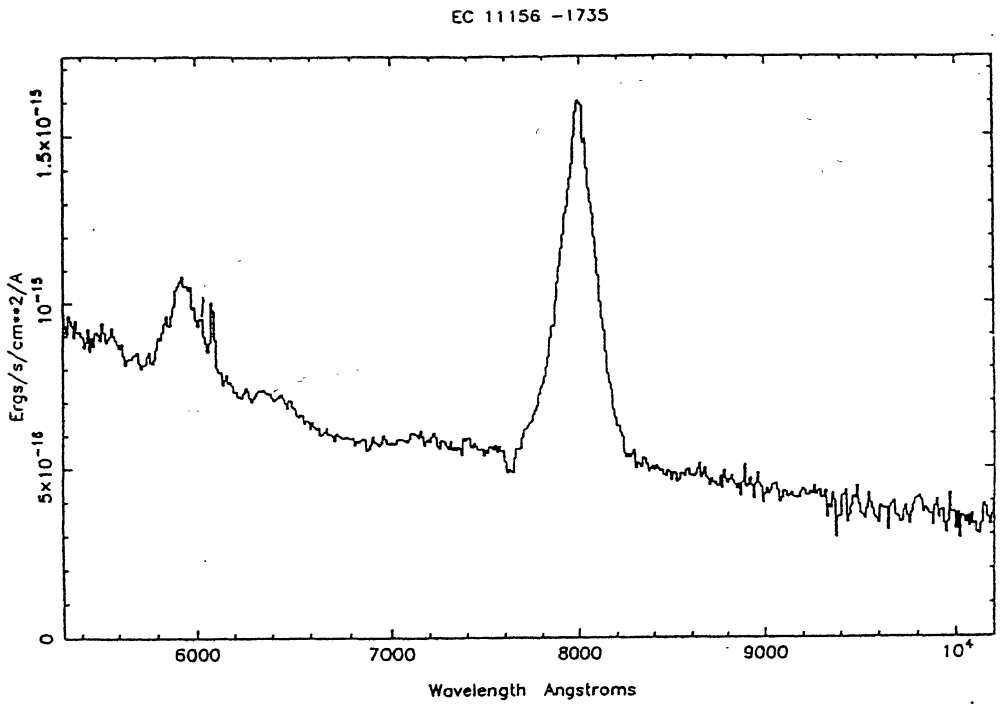

Figure 13. Red spectrogram of QSO ($z=0.220$) in Fig. 12(c) taken with the AAT FORS spectrograph.

is achieved using an observation of a spectrophotometric standard star obtained during the night. Both counts and flux spectra are retained. Examples of the flux-calibrated spectrograms for a wide variety of EC objects are shown in Figs 9–14.

4.2 Classification of spectra

Initially all the EC spectra were classified 'on-line', that is, by simply making an estimate of the spectral type at the telescope. With the Reticon system it is possible to see the incoming spectrograms building up in flat-field-corrected and sky-subtracted form and also with varying amounts of smoothing. It is also possible to co-add spectrograms to improve the signal-to-noise ratio, especially as the Reticon being a photon-counting device has essentially zero readout noise. This initial classification process proved very useful for selecting objects for further study and also, where spectrograms could not be immediately classified, to carry out further observations. For example, poor signal-to-noise spectrograms were often repeated and then the data co-added; in some cases the spectrum appeared featureless and we were able to try spectroscopy at lower dispersion (210 Å mm^{-1}; ~8-Å resolution) but with increased spectral range (~3600–7000 Å). In some cases, it has proved possible to obtain data from the Mount Stromlo and Siding Spring Observatory 2.4-m telescope and from the 3.9-m Anglo-Australian Telescope plus the FORS spectrograph – compare the spectrograms of EC 11156 – 1735 in Figs 12 and 13, for example.

Before any results are published, we plan to reclassify all objects. This has already been done for the first zone independently by two of the authors (DK and DOD), and the independent classifications have been compared and, where differences occur, the spectrograms have been re-examined. The reclassifications have been carried out by comparison with spectrograms of known objects observed with the same configuration as for the EC Survey and also by using the criteria of Moehler et al. (1990). In the first case, we have obtained spectrograms of mainly bright stars (HR) covering types from late-O to mid-F, as well as some of the brighter horizontal branch stars; in the second case, we have tried to segregate the evolved objects using the classes proposed by Moehler et al. (1990), which are discussed in more detail below.

Fig. 9 shows three hot 'B' type stars and an F star. The F star is easily identifiable by the strong H and K lines of Ca II and the G-band feature at $\lambda \sim 4300$ Å. We have attempted to classify these objects relative to the spectra of normal F stars, but it is quite likely that many of the EC stars are late-type subdwarfs (as evidenced by the $U-B$ 'excesses'), and errors might occur because of the metal-deficiency in these objects. The 'B' stars can be separated on the basis of the Balmer jumps. Hot subdwarfs (sdB) typically have rather broad H lines visible up to only $n=10$ to 12; normal B stars have Balmer series visible to $n=12$ to 14, and the blue horizontal branch stars (HBB in Moehler et al.) may have even higher members of the Balmer series visible in our spectrograms. Moehler et al. (1990) also find weak Mg II (4481 Å) in the HBB stars and use He I (4388 Å) ~ He I (4471 Å) as an indicator of 'normal B', and He I (4471 Å) $\gg$ He I (4388 Å) as an indicator of sd/HBB types. We have used this criterion, but have examples where He I 4388 is apparently quite strong in obvious subdwarfs, so the Balmer jump has been a factor in our classification process. A further problem is that, particularly for stars fainter than about 16 mag, we have not always been able to achieve a high enough signal-to-noise ratio (despite co-adding spectrograms, for example) to make a definitive classification. In such cases, a spectral type of say ~B5/HBB? will indicate

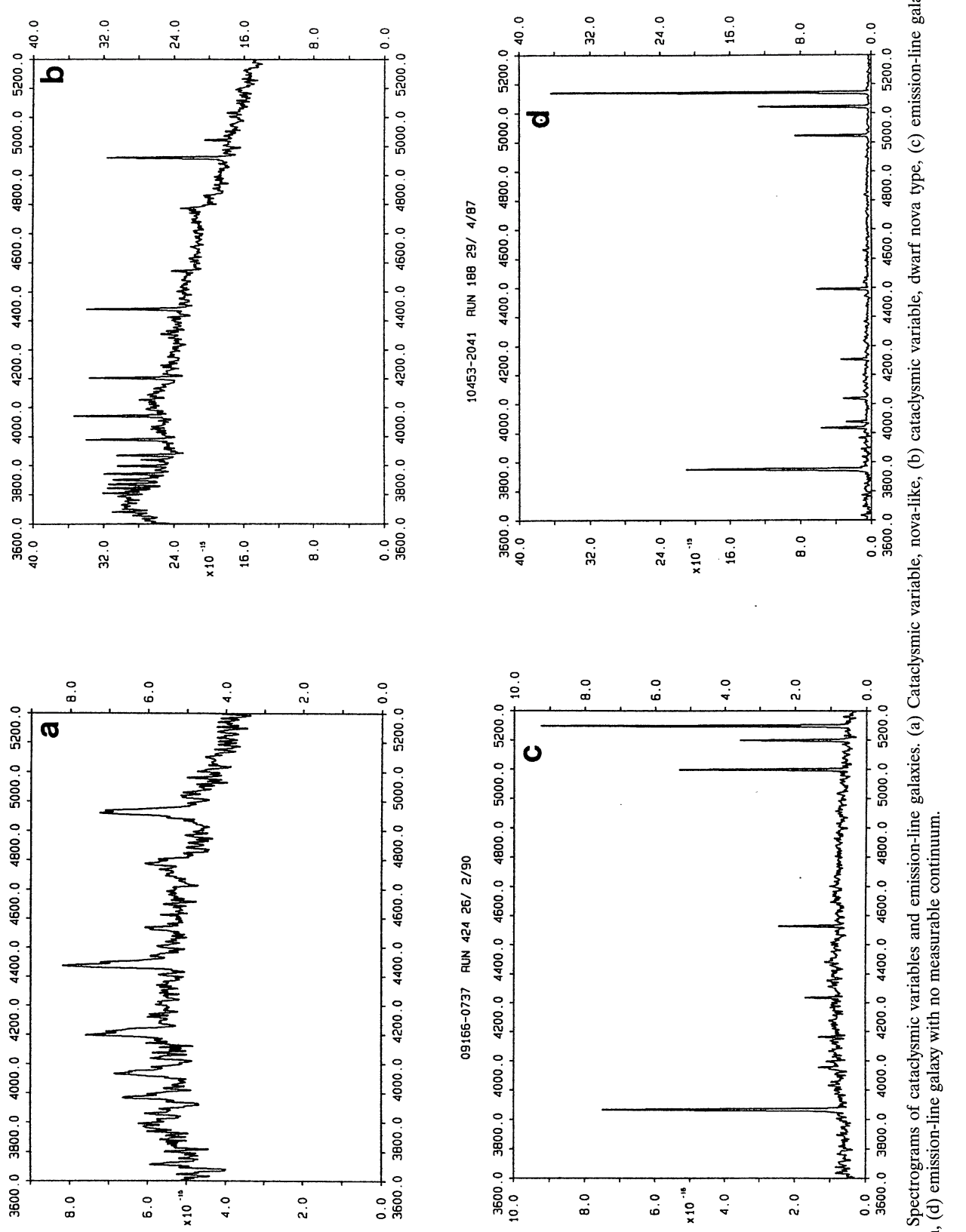

Figure 14. Spectrograms of cataclysmic variables and emission-line galaxies. (a) Cataclysmic variable, nova-like, (b) cataclysmic variable, dwarf nova type, (c) emission-line galaxy with continuum, (d) emission-line galaxy with no measurable continuum.

that we have classified the star as B5, but there remains uncertainty and the star could be an HBB type. In Fig. 9(c), the early B star is one of a group of apparently normal (high-mass) B stars which have been found at high galactic latitudes and hence large distances from the Galactic plane (Kilkenny et al. 1991, 1995).

Fig. 10 shows a selection of hot subdwarfs. All these stars have similar *UBV* colours, although they cover a wide range of temperature and chemical abundance. We have used the Moehler et al. (1990) classification scheme (see this reference for more details and for notes on the 'historical' development of the scheme). In brief, the 'sd' stars show broad Balmer absorption lines, and the subdivisions are defined by:

sdB – weak (or no) He I in absorption,
sdOB – weak He I and He II (4686 Å) in absorption,
sdO – He II in absorption.

As noted above, in the first two classes, typically He I (4471 Å) is much stronger than He I (4388 Å). The types He-sdB and He-sdO have no detectable hydrogen absorption, but have strong He I plus weak He II (He-sdB) or strong He II and sometimes weak He I (He-sdO). In the case of He-sdO stars, Pickering series He II lines appear at similar wavelengths to the Balmer series lines of hydrogen.

Fig. 11 shows a sample of white dwarf spectrograms. These stars are obviously distinguishable from lower gravity objects by the large width of the Balmer lines which are visible to typically only $n=8$. Note that a high signal-to-noise ratio is needed to recognize the very hot objects which have weak features (e.g., bottom right in Fig. 11d). For white dwarfs, we have followed the classification scheme of Sion et al. (1983), illustrated in the atlas of Wesemael et al. (1993). The DA white dwarfs dominate with smaller numbers of DO and DB, and other kinds of white dwarfs are also being discovered in the EC Survey.

Fig. 12 illustrates the wide variety of spectral characteristics exhibited by quasi-stellar objects (QSOs) in the survey. Because of the ultraviolet-excess criterion, any QSOs discovered are almost certainly of redshift $z<2.3$. A few high-redshift QSOs with $z\sim2$ have been discovered with the emission lines of Lyman α and C IV redshifted into the optical domain. The majority of the QSOs are low-redshift systems ($z\lesssim0.5$) with the emission lines of the Balmer series visible. One object had no obvious emission or absorption lines in its spectrum and appeared as a continuum. However, a spectrum obtained with the FORS spectrograph on the Anglo-Australian Telescope (Fig. 13) for $5500<\lambda<10\,000$ Å showed clearly that it was a low-redshift ($z=0.22$) QSO with strong Hα and Hβ Balmer emission. A group of very interesting QSOs with narrow absorption lines of low-excitation Fe II and Mg II has been found. In some cases multiple redshift systems have been found, presumably as a result of intervening clouds in the line of sight to the QSO. The importance of these QSOs is that they are all relatively bright ($B\lesssim16.5$) and excellent candidates for high-dispersion spectroscopy.

Of the total number of QSOs found in the survey so far ($\sim$100 QSOs) only 16 per cent are in the catalogue of known QSOs (Hewitt & Burbidge 1993), and a further 6 per cent are in the catalogue of extragalactic emission-line objects similar to QSOs (Hewitt & Burbidge 1991). This illustrates the great incompleteness in southern hemisphere searches for bright QSOs and active galactic nuclei.

Fig. 14 illustrates four other emission-line objects. The two upper panels are cataclysmic variables with broad Balmer emission lines. These emission lines arise from the accretion disc surrounding the compact object, and one spectrum shows evidence of a double-peak structure as expected for a system viewed nearly edge-on. The two lower panels are emission-line galaxies with spectra like those of extragalactic H II regions. The lines are the forbidden lines of oxygen and the Balmer series of hydrogen, and in one case there is almost no continuum. Although galaxies were excluded in the star/galaxy discrimination, examination of the plates has shown that these objects have such a bright nucleus that they appear star-like on the Schmidt photographs.

5 SURVEY COMPLETENESS

It is important to establish the completeness of a survey for the purposes of comparison with other surveys and for statistical analysis of classes of objects. In the following we determine the B magnitude and $(U-B)$ colour limits of the survey and estimate the internal completeness. The external completeness (e.g., by comparison with the PG Survey in the zone of overlap) will be discussed in a separate paper (Kilkenny et al. 1997).

5.1 Number–magnitude counts of paired data

Fig. 15 shows the differential number–magnitude counts for the unpaired B data and the paired U and B data. Because the B plate is much deeper than the U plate, it is the U plate that effectively sets the limit to the number of objects that pair. With a 15-min exposure for the B plate the magnitude limit is $B\sim20$. Most of the very faint red images on the B plate, however, are not detectable on the U plate and thus are lost in the pairing. The effect of the magnitude limits of both plates can be seen in the colour–magnitude diagram (Fig. 2). The B-plate limit (as determined by a COSMOS area cut of 10 pixel) appears as the upper horizontal limit to the distribution of points at BMAG~-800. The U-plate limit appears as the upper sloping limit to the distribution, showing that successively redder images are lost in the pairing at successively brighter B magnitudes.

An estimate of the depth of the EC Survey can be obtained from the expected number of stars in the galaxy brighter than $B=18$ predicted by the Bahcall & Soneira (1980) galaxy model for the galactic latitude and longitude of the field. The predicted number counts show that the paired data are effectively complete (at least at blue colours) to much fainter than $B=18$. This can also be seen in Fig. 2, where the ultraviolet strong objects are detected in the paired data to magnitude $B\sim20$. Despite the apparent completeness of the photographic catalogue, a small percentage of brighter objects do not pair. This is investigated in more detail in the next section.

5.2 Completeness of image pairing and doubles

It is necessary to establish the completeness of the pairing of the U and B plates. There are a number of reasons as to why

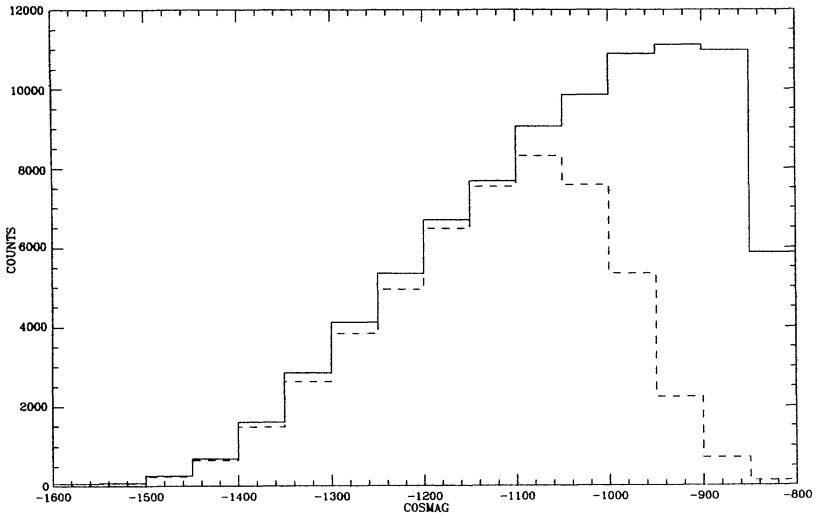

Figure 15. The differential number–magnitude counts as a function of Cos B for the B plate (solid line) and for the paired U, B data (dashed line).

an image may not successfully pair, e.g., an image counted as two separate images on one plate but a merged double on the other, satellite or asteroid trails intersecting an image, emulsion flaws. These effects can lead to non-pairing if, as a result, the image position on the U and B plates is outside the permitted error box for successful pairing.

The magnitude of this effect was estimated by examining two fields of differing star density. Both fields were at galactic latitude $-33°$ with one field towards the Galactic Centre and one towards the anticentre. The B-plate star density down to $B=20$ varied from 1926 to 5432 stars per square degree, with the U-plate density being much lower. The majority of EC Survey B plates have star densities within this range. For each field a central area covering at least 1000 objects was examined visually in detail, and reasons for non-pairing noted. In order to avoid incompleteness arising from faint objects visible on one plate and not the other, the completeness estimation was restricted to all objects on the B plate with BMAG < -1000 (corresponding to $B \sim 18$).

In addition to the completeness of the pairing, we also determined the percentage of doubles or multiples that were rejected. The reason for rejection is that any object found as a double or multiple has to be rejected as a candidate blue object, since the photometry is unreliable as a consequence of the non-linear response of the photographic emulsion. Doubles closer than a certain critical separation will be counted as a single merged object. Beyond this separation a double will be counted as two singles. In between there is a range of separations where an image can appear as a single merged image on one plate and two separate images on the other. In practice, at the scale of UKST plates, it was found that stars with a characteristic separation of 8–12 arcsec were likely to have this problem, although clearly this separation will be a function of the magnitude and the point-spread function.

If we count both images that did not pair and images that were doubles or multiples, then the total percentage of images rejected was 3.4 per cent in the low star density field and 4.7 per cent in the high density star field. As most of the survey fields occur in this star density range, it can be concluded that to $B \sim 18$ the survey completeness as regards loss of paired images and rejection of doubles/multiples is 95 per cent.

Table 3. Duplicate plate pairs and selection of blue objects with $B < 16.5$.

Field no.	Plate pair	Common	Not in common		
			F/G	A	B/bhb
503	UB10694	6	12	1	1
	UB12577	6	1	0	0
640	UB11613	12	6	0	0
	UB12474	12	0	0	0
710	UB11819	11	6	0	0
	UB12351	11	1	1	0

5.3 Blue object selection completeness

The 'internal' completeness has been determined in two separate ways: (i) by comparing the results for duplicate U, B plate pairs of the same field, and (ii) by examining the overlap region between plate pairs in different fields.

Duplicate plate pairs exist for three fields. The results are presented in Table 3. As the magnitude limits may differ between the two selections, the total number of blue objects identified and the number in common do not give a true measure of the statistics. Thus the statistics presented have been restricted to objects with $B < 16.5$, as these are objects for which we have both photometry and spectroscopy. This also enables us to examine the spectral type of the objects not in common. It can be seen that the objects not in common are nearly all F/G-type stars, the remainder being early-type stars. This shows that objects of spectral type earlier than F/G are found to be common to both selections, and that the objects not in common are, by and large, stars of later spectral type. Thus the main reason for the difference in blue object selections is the non-Gaussian error

distribution in photographic magnitudes (Section 3.3) causing a small percentage of F/G-type stars to be selected spuriously as candidate blue stellar objects.

The second method of determining the 'internal' completeness was to examine the regions of plate overlap in different fields, defined by the plate centres and area measured by COSMOS. Within this RA, Dec. overlap region the two blue object selections were compared for the common and non-common objects. The completeness calculation follows the procedure of Green et al. (1986). Let a be the number of objects found twice, and b be the number of objects found once. Then if p is the probability of finding a blue object in a single plate pair, $p=2a/(2a+b)$. The completeness, c, of the survey is the sum of the fraction of objects found once in the non-overlap region, the fraction of objects found twice in the overlap region, and the fraction of objects found once in the overlap region. If f is the fraction of the total area surveyed which lies in an overlap region, then $c=(1-f)p+f[p^2+2p(1-p)]$. Note that triple overlaps are neglected in this calculation. Provided that we considered only fields with *UBV* photoelectric photometry and objects brighter than $B=16.5$, this enables the completeness of the survey to be defined as a function of $U-B$ colour. In practice, 70 fields with a coverage of 2002 deg^2 were used to evaluate the survey completeness. These fields provided 88 overlap regions with total coverage of 211 deg^2, i.e., $f=0.1$.

Fig. 16 illustrates, as a function of $U-B$ colour, this 'internal' completeness and the number of objects found only once in the overlap region. It is clear that the objects found only once are predominantly redder objects, as one would expect since the selection of these objects is sensitive not only to the non-Gaussian error statistics but also to the location of the red boundary, which may vary slightly from field to field (as it is determined from the uncalibrated photographic magnitudes). It is also apparent that the effective colour cut-off for the survey is $U-B<-0.4$. Bluer than this the survey is 94 per cent complete. It is noticeable that a small percentage of very blue objects (e.g., $U-B<-1.0$) is found only once. One reason for the loss of some blue objects is images on the U and B plates which do not pair and thus are not in the merged catalogue.

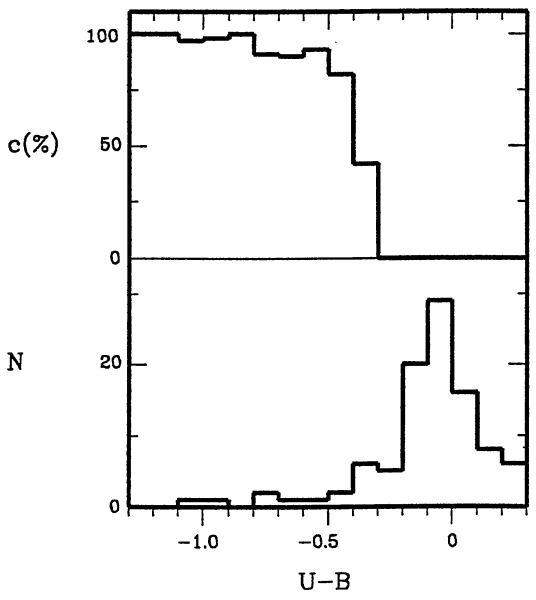

Figure 16. From plate overlap regions, (a) the internal completeness of the survey, (b) the number of objects found only once, both as a function of photoelectric $U-B$ colour.

5.4 The EC Survey B and $U-B$ limits and completeness

To summarize, the EC Survey is photographically complete to $B\sim18$. Photoelectric photometry is being obtained for all objects brighter than $B=16.5$, and from this we know that the colour cut-off is selecting objects with $U-B<-0.4$. The limit of $B=16.5$ is reached by ordering the objects in decreasing COSMOS B brightness and observing photoelectrically until a magnitude of $B=16.5$ is observed. As described in Section 5.2, a small percentage of objects (4 per cent) is lost in the pairing of the U and B plate catalogues and the rejection of merged images at the visual inspection stage. Of the paired single-image objects we know that the survey is 94 per cent complete for $B<16.5$ and $U-B<-0.4$. These incompleteness corrections need to be applied if one is using the survey for statistical purposes, such as the space density of objects.

6 PUBLICATION AND STATUS OF SURVEY

Because of the long time-scale required to complete the survey it was considered best to publish it as a series of papers covering galactic latitude zones as described in Table 4. These zones essentially include the area of sky with $|b|>30°$ not covered by the PG Survey. A field is included in a zone if the plate centre satisfies the declination and galactic longitude limits in Table 4. The total number of fields is 391, where we have excluded 11 fields in the Large and Small Magellanic Clouds because the image analysis would not be valid in such crowded fields. The zones in Table 4 are listed in order of decreasing priority. A decision still has to be made as to whether or not zone 7 will finally be included.

The status of the EC Survey is summarized in Table 5. Of the 391 fields in the survey, 251 (64 per cent) have U,B plate

Table 4. Zoning of Edinburgh–Cape Blue Object Survey.

Zone	Declination (field centres)	Galactic Latitude	Number of UK Schmidt fields
1	$\delta\le-15°$	b $>+30°$	61*
2†	$\delta\le-15°$	$-40°<$ b $<-30°$	62
3†	$\delta\le-15°$	$-50°<$ b $<-40°$	53
4	$\delta\le-15°$	$-60°<$ b $<-50°$	52
5	$\delta\le-15°$	$-70°<$ b $<-60°$	45
6	$\delta\le-15°$	$-80°<$ b $<-70°$	48
7	$-10°\le\delta\le0°$	b $<-30°$	70

†The Large and Small Magellanic Cloud fields (UK Schmidt Telescope field numbers 28, 29, 30, 33, 51, 55, 56, 57, 84, 85, 86) have been excluded from zones 2 and 3.
*The North Galactic Cap zone contains some fields outside the specified declination and galactic latitude limits, primarily to aid in comparison with the PG Survey.

Table 5. Status of the EC Survey as at 1996 October 1.

Zone	Number of fields	U,B plate pairs taken	Measured in COSMOS	Blue object selection
1	61	61	61	61
2	62	61	58	53
3	53	41	25	19
4	52	41	22	16
5	45	20	19	15
6	48	22	21	18
7	70	5	5	2
Total	391	251	211	184

pairs and 184 (47 per cent) have been digitized and analysed to extract the blue stellar objects. In comparison with the PG Survey, which had a number density of objects of 0.2 per square degree, the EC Survey is finding a number density of 2 per square degree. This greater number density is primarily because of the fainter magnitude limit ($B \sim 18$), compared with the PG limiting magnitude of $B \sim 16$. The number of stars with $B < 16.5$ in the whole survey is expected to be ~ 5000, giving a number density of 0.5 per square degree. Of these brighter stars, *UBV* photoelectric photometry has been obtained for 2025 stars, and spectroscopy for 1832 stars.

The zones to be published will include details only on stars brighter than $B = 16.5$, listing coordinates accurate to 1 arcsec, *UBV* photoelectric photometry and spectral classification of each object. The objects fainter than $B = 16.5$ to the limit of the blue object selection will not be published, but will be maintained as a data base of photographically selected ultraviolet-strong stellar objects. It is expected that some of these fields will be followed up to obtain photometry and spectroscopy with larger telescopes and to study the nature of the fainter objects.

ACKNOWLEDGMENTS

The Edinburgh–Cape Survey is based on data obtained with the UK Schmidt Telescope at the Anglo-Australian Observatory, measurements made using the COSMOS facility at the Royal Observatory, Edinburgh, and data obtained at the South African Astronomical Observatory. The success of a survey on such a large scale would not be possible without the support of many people. We especially thank M. W. Feast, the former Director of SAAO, for allocating substantial amounts of telescope time for the follow-up photometry and spectroscopy.

REFERENCES

Bahcall J. N., Soneira R. M., 1980, ApJS, 44, 73
Beard S. M., MacGillivray H. T., Thanisch P. F., 1990, MNRAS, 247, 311
Blair M., Gilmore G., 1982, PASP, 94, 742
Buckley D. A. H., O'Donoghue D., Kilkenny D., Stobie R. S., Remillard R. A., 1992, MNRAS, 258, 285
Chen A., O'Donoghue D., Stobie R. S., Kilkenny D., Roberts G., van Wyk F., 1993, in Kilkenny D., Lastovica E., Menzies J. W., eds, Precision Photometry. South African Astronomical Observatory, p. 200
Demers S., Kibblewhite E. J., Irwin M. J., Nikathorn D. S., Béland S., Fontaine G., Wesemael F., 1986, AJ, 92, 878
Gilmore G., 1983, in Stobie R. S., McInnes B., eds, Occ. Rep. R. Obs. Edinburgh No. 10, Workshop on Astronomical Measuring Machines, p. 259
Green R. F., Schmidt M., Liebert J., 1986, ApJS, 61, 305
Hewitt A., Burbidge G., 1991, ApJS, 75, 297
Hewitt A., Burbidge G., 1993, ApJS, 87, 451
Kilkenny D., O'Donoghue D., Stobie R. S., 1991, MNRAS, 248, 664
Kilkenny D., Luvhimbi E., O'Donoghue D., Stobie R. S., Koen C., Chen, A., 1995, MNRAS, 276, 906
Kilkenny D., O'Donoghue D., Koen C., Stobie R. S., Chen A., 1997, MNRAS, 287, 867 (this issue)
Koen C., O'Donoghue D., Stobie R. S., Kilkenny D., Ashley R., 1995, MNRAS, 277, 913
MacGillivray H. T., Stobie R. S., 1984, Vistas Astron., 27, 433
Menzies J. W., Cousins A. W. J., Banfield R. M., Laing J. D., 1989, SAAO Circ., 13, 1
Menzies J. W., Marang F., Westerhuys J. E., 1990, SAAO Circ., 14, 33
Moehler S., Richtler T., de Boer K. S., Dettmar R. J., Heber U., 1990, A&AS, 86, 53
O'Donoghue D., Chen, A., Kilkenny D., Stobie R. S., 1993, in Barstow M., ed., Proc. 8th European Workshop on White Dwarf Stars. Kluwer, Dordrecht, p. 37
O'Donoghue D., Stobie R. S., Chen A., Kilkenny D., Koen C., 1993, in Kilkenny D., Lastovica E., Menzies J. W., eds, Precision Photometry. South African Astronomical Observatory, p. 72
O'Donoghue D., Kilkenny D., Chen A., Stobie R. S., Koen, C., Warner B., Lawson W. A., 1994, MNRAS, 271, 910
Reid N., Gilmore G., 1982, MNRAS, 201, 73
Savage A., Cannon R. D., Stobie R. S., Kilkenny D., O'Donoghue D., Chen A., 1993, Proc. Astron. Soc. Aust., 10, 265
Sion E. M., Greenstein J. L., Landstreet J. D., Liebert J., Shipman H. L., Wegner G. A., 1983, ApJ, 269, 253
Stobie R. S., 1986, Pattern Recognition Lett., 4, 317
Stobie R. S., Henley R. C., 1983, in Stobie R. S., McInnes B., eds, Occ. Rep. R. Obs. Edinburgh No. 10, Workshop on Astronomical Measuring Machines, p. 49
Stobie R. S., Ishida K., 1987, AJ, 93, 624
Stobie R. S., Morgan D. H., Bhatia R. K., Kilkenny D., O'Donoghue D., 1988, in Davis Philip A. G., Hayes D. S., Liebert J. W., eds, Proc. IAU Coll. 95: The Second Conference on Faint Blue Stars. L. Davis Press, Schenectady, p. 493
Stobie R. S., Chen A., O'Donoghue D., Kilkenny D., 1992, in Warner B., ed., ASP Conf. Ser. Vol. 30, Variable Stars and Galaxies. Astron. Soc. Pac., San Francisco, p. 87
Stobie R. S., Chen A., O'Donoghue D., Kilkenny D., 1993, MNRAS, 263, L13
Stobie R. S., O'Donoghue D., Ashley R., Koen C., Kilkenny D., 1995, MNRAS, 272, L21
Wallace P. T., Tritton K. P., 1979, MNRAS, 189, 115
Wesemael F., Greenstein J. L., Liebert J., Lamontagne R., Fontaine G., Bergeron P., Glaspey J. W., 1993, PASP, 105, 761
Yoshii Y., Ishida K., Stobie R. S., 1987, AJ, 93, 323